This is the author's version of the article published in Colloids and Surfaces B: Biointerfaces. Changes were made to this version by the publisher prior to publication. The final version is available at 10.1016/j.colsurfb.2024.114342

Bioactive Dextran-based Scaffolds from Emulsion Templates Co-Stabilized by Poly(lactic-*co*-glycolic acid) Nanocarriers.

Maude Ducrocq[a, b, c], Arianna Rinaldi[b], Boris Halgand[c], Joëlle Veziers[c], Pierre Guihard[c*], Frank Boury[b*], Antoine Debuigne[a*]

[a] Center for Education and Research on Macromolecules (CERM), CESAM Research Unit, Chemistry Department, University of Liège (ULiege), Quartier Agora, 13 Allée du Six Août, Sart-Tilman, B-4000 Liège, Belgium.

[b] Université d'Angers, INSERM, CNRS, CRCI2NA, F-49000, Angers, France.

[c] Nantes Université, Oniris, Univ Angers, CHU Nantes, INSERM, Regenerative Medicine and Skeleton, RMeS, UMR 1229, F-44000 Nantes, France

*Corresponding authors: Antoine Debuigne adebuigne@uliege.be, Frank Boury frank.boury@univ-angers.fr, Pierre Guihard pierre.guihard@univ-nantes.fr

Graphical abstract.

This is the author's version of the article published in Colloids and Surfaces B: Biointerfaces. Changes were made to this version by the publisher prior to publication. The final version is available at 10.1016/j.colsurfb.2024.114342

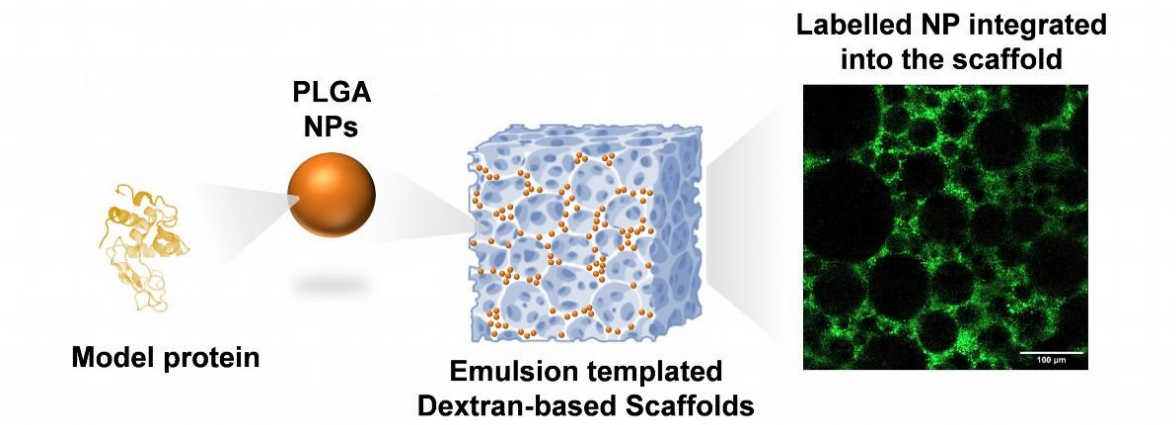

Abstract. Porous polymer scaffolds are widely investigated as temporary implants in regenerative medicine to repair damaged tissues. While biocompatibility, degradability, mechanical properties comparable to the native tissues and controlled porosity are prerequisite for these scaffolds, their loading with pharmaceutical or biological active ingredients such as growth factors, in particular proteins, opens up new perspective for tissue engineering applications. This implies the development of scaffold loading strategies that minimize the risk of protein denaturation and allow to control their release profile. This work reports on a straightforward method for preparing bioactive dextran-based scaffolds from high internal phase emulsion (HIPE) templates containing poly(lactic-co-glycolic acid) (PLGA) nanoparticles (NPs) serving both as co-stabilizers for the emulsion and nanocarriers for drug or therapeutic protein models. Scaffold synthesis are achieved by photocuring of methacrylated dextran located in the external phase of a HIPE stabilized by the NPs in combination or not with a non-ionic surfactant. Fluorescent labelling of the NPs highlights their integration in the scaffold. The introduction of NPs, and even more so when combined with a surfactant, increases the stability and mechanical properties of the scaffolds. Cell viability tests demonstrate the non-toxic nature of these NPs-loaded scaffolds. The study of the release of a model protein from the

scaffold, namely lysozyme, shows that its encapsulation in nanoparticles decreases the release rate and provides additional control over the release profile.

Highlights:

- A model protein is encapsulated in PLGA nanoparticles by a non-denaturing process.
- Macroporous scaffolds are produced from emulsions co-stabilised by nanoparticules.
- Nanoparticles serve both as emulsion stabilizers and protein nanocarriers.
- Nanoparticles-loaded scaffolds do not exhibit toxicity.
- Protein incorporation within particles embedded in scaffolds prolongs the release.

Keywords :

Emulsion templates; nanoparticles; protein encapsulation; bioactive scaffolds; protein release; tissue engineering.

Statistics : 5500 words, 1 table + 7 figures.

1. Introduction

Tissue engineering (TE) has emerged as a groundbreaking field that aims to regenerate damaged or diseased tissues and organs by combining principles of biology and material science. A key aspect of TE is the design of scaffolds that mimic the natural extracellular matrix and provide a supportive framework for cell growth, proliferation, and differentiation. Porous polymer scaffolds with a three-dimensional interconnected structure, resembling the native tissue architecture, are commonly used for TE and allow nutrient diffusion, waste removal and cellular integration, essential for tissue regeneration. The degradability and biocompatibility of these porous scaffolds are prerequisites to ensure compatibility with the host tissue and the ability to degrade over time as new tissue forms. Growth factors, such as Bone Morphogenetic Proteins (BMPs) and Vascular Endothelial Growth Factor, are also considered as additives for these implants to stimulate the cellular activities, fostering enhanced tissue integration and regeneration.

An emerging method of scaffold manufacturing for TE relies on high internal phase emulsion (HIPE) templating polymerization [1,2]. This approach entails the initial formation of a HIPE, wherein the internal droplet phase exhibits a volume fraction higher than 74% and the continuous external phase contains the polymer matrix precursor. Subsequently, the outer phase is cured to fix the emulsion microstructure before removal of the droplet phase to unveil the desired porosity. The polymerization step also allows the formation of pores between the inner phase droplets through interfacial destabilization, which often occurs at the thinnest points of the outer phase film surrounding the droplets. The resulting polymerized HIPEs (polyHIPEs) feature a hierarchically structured and three-dimensionally interconnected morphology, consisting of quasi-spherical cavities connected by circular holes called windows whose sizes vary from one to a few hundred micrometers. The morphology of polyHIPEs can be readily

tailored by finely adjusting the type and concentration of the surfactant, as well as controlling the volume ratio of emulsion phases and optimizing the curing process [3–5]. Emulsion-templated porous materials, comprising acrylate-based polymers [6–9], polyethylene glycol [10,11], polyesters[12–14], polyurethanes [15], polysaccharides [16–18], gelatin [19,20], or peptides [21], have been investigated as scaffolds for TE applications.

Among the different types of emulsions, Pickering emulsions are notable for their exceptional stability and notably emerged as valuable templates for the fabrication of advanced scaffolds, as discussed hereafter. These emulsions achieve excellent stability through particles strongly adsorbed onto the droplet surfaces, which form a protective layer that prevents coalescence by steric repulsions. Numerous nanoparticles (NPs) have been considered as stabilizers for Pickering emulsions, including biocompatible and natural particles, especially in the perspective of their use in the biomedical field [22–27]. Pickering emulsifiers are also employed for the stabilization of HIPEs [28,29] and the production of interconnected macroporous polyHIPEs [30–33]. In comparison to emulsion templating methods based on conventional surfactants, Pickering HIPE polymerizations require a reduced quantity of stabilizer and yield more stable emulsions. Nevertheless, polyHIPEs derived from Pickering emulsions exhibit occasionally moderate to low interconnectivity requiring the use of a co-surfactant to achieve an adequat degree of openness [28–31]. In the last years, polymer scaffolds with enhanced structural integrity and tailored functionalities were produced by Pickering HIPE emulsion. For instance, open-cell polyacrylamide-based scaffolds allowing adsorption and growth of the HepG2 cells were produced via gelatin NP-stabilized HIPE templates [34]. Gelatin NPs also served with gelatin as co-stabilizer of oil/water (O/W) HIPEs used in the production of interconnected hierarchical porous protein scaffolds demonstrating degradability, biocompatibility as well as adhesion and growth of L929 cells [35]. Citric acid crosslinked

starch NPs provided good stabilization of emulsion-template for the preparation of acrylamide-based supports for cell culture [36]. Biodegradable scaffolds composed of poly(L-lactic acid) (PLLA) and poly(ε-caprolactone) (PCL) were created via solvent evaporation of 3D-printed Pickering HIPEs stabilized by hydrophobically modified silica NPs [37]. Alternatively, freeze-drying of 3D printed Pickering HIPEs, stabilized by hydroxyapatite and silica NPs, resulted in scaffolds based on poly(D,L-lactide) exhibiting shape memory properties and enhanced biomineralization capabilities [38]. Finally, Pickering emulsions stabilized by PLLA-grafted hydroxyapatite NPs (HAp) led to PLGA [39] and PCL [40] polyHIPEs including 3D-printed ones [41], able to promote the adhesion and proliferation of bone mesenchymal stromal cells (BMSCs) [39–41]. Furthermore, a nonsteroidal anti-inflammatory drug was successfully loaded into the polyester matrices of these bioactive scaffolds which displayed sustained release profiles likely to address the anti-inflammatory requirements for scaffold implantation [39–41].

This work reports a straightforward method for designing dextran-based scaffolds from emulsion templates co-stabilized by polyester nanocarriers in the perspective of their use as bioactive scaffolds for TE application. A distinctive feature of this contribution lies in the dual role of the NPs serving as co-stabilizers for the emulsion and reservoirs for active pharmaceutical ingredients (API). Compared to the direct incorporation of the APIs into the matrix of the scaffolds, encapsulating the active principle within the particles themselves embedded in the scaffold is expected to afford additional control of the release profile and to limit burst release effect. As a nanocarrier and emulsion co-stabilizer, we considered PLGA/PEG-PLGA NPs produced by a non-denaturing phase separation method utilizing non-toxic solvents in the form of glycofurol and isosorbide dimethyl ether [42]. This approach demonstrates the efficient encapsulation of several drug models or therapeutic proteins such as lysozyme, stromal cell-derived factor 1-α, BMP-2 and BMP-4, as well as their sustained release

[43–45]. As illustrated in Figure 1, the macroporous dextran-based scaffolds were then produced via photocuring of methacrylated dextran in a dodecane-in-water HIPE stabilized by the NPs in combination or not with a non-ionic surfactant (F-68). The influence of the nature of the co-stabilizers on the morphology and mechanical properties of the polyHIPEs was studied. The effective integration of PLGA/PEG-PLGA NPs into the dextran-based scaffold was evaluated through confocal microscopy. Comprehensive indirect cell viability assessments were performed to validate the non-toxic nature of these scaffolds. As a proof of concept, such polyHIPEs were formulated using NPs loaded with a model protein, lysozyme, and *in vitro* studies were carried out to assess the sustained release profile of the protein.

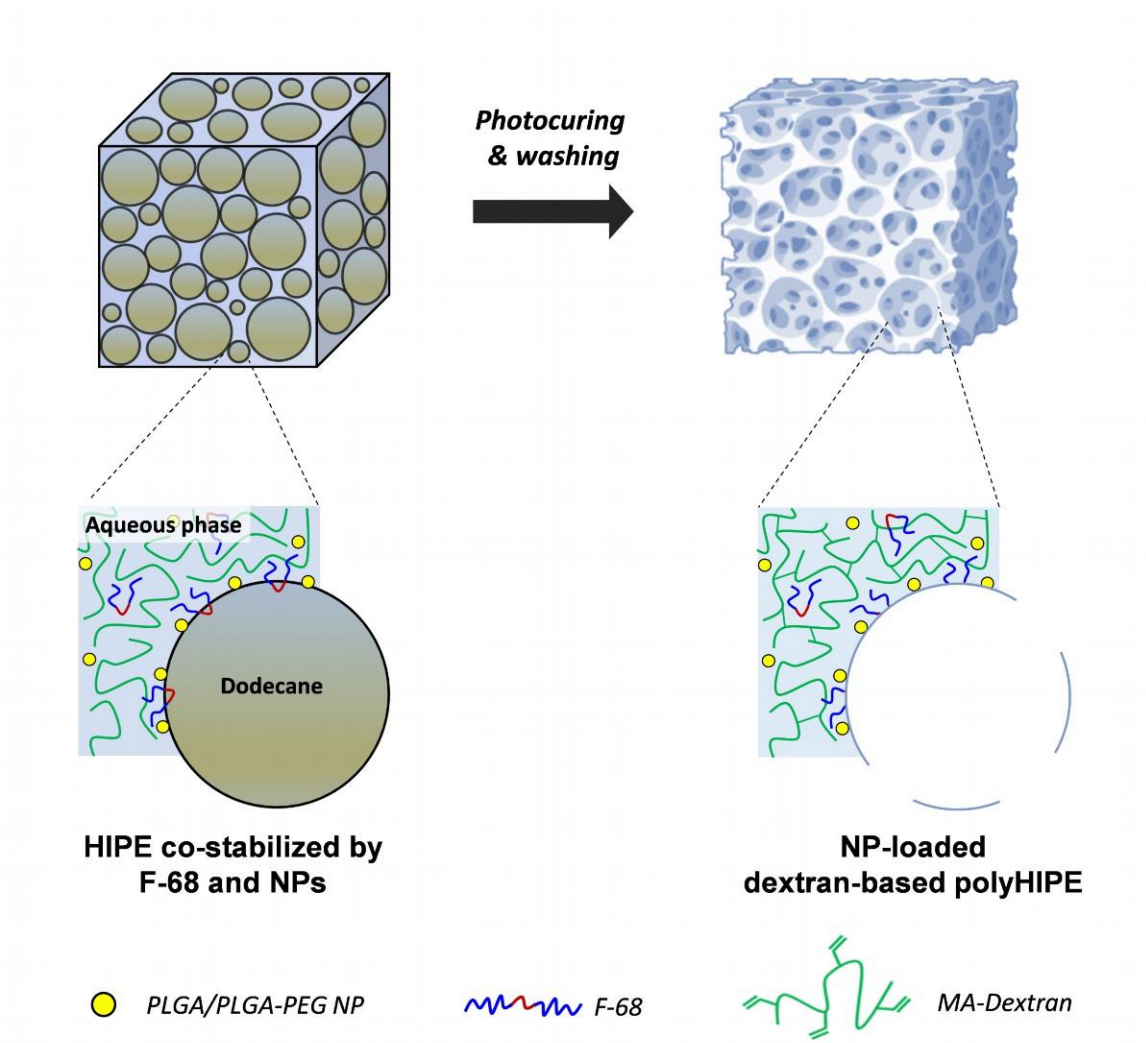

Figure 1. General strategy for the synthesis of NPs-loaded scaffolds by emulsion templating polymerization.

2. Materials and methods

2. 1. Materials

Lithium phenyl-2,4,6-trimethylbenzoylphosphinate (LAP, >95%,), Kolliphor® P 188 (F-68), isosorbide dimethyl ether, bovine serum albumin, glycofurol (also named tetraglycol), lysozyme from chicken egg white, *Micrococcus lysodeikticus*, were purchased from Sigma-Aldrich (Saint-Louis, Missouri, USA). Isosorbide dimethyl ether (DMI), dimethyl sulfoxide (DMSO), DMEM (Dulbecco's Modified Eagle Medium), Penicillin-streptomycin (10 000 U/ml), Cell counting Kit-8, ADNdb Quant-iT™ PicoGreen Kit and PBS (Phosphate buffered saline - pH 7.2) were purchased from Thermo Fisher Scientific (Waltham, Massachusetts, USA). Fetal Bovine Serum was purchased from Dominique Dutscher (Bernolsheim, France). Dodecane (>99%) was purchased from TCI chemicals (Tokyo, Japan). Spectra/Por® 7 pre-treated reconstituted cellulose tubing with a molecular cutoff of 3.5 kDa were used. Unless specified otherwise, all chemicals were analytical grade and used as received and Milli-Q water was used.

2. 2. Polymer synthesis and characterization

Synthesis and characterization of PLGA, PEG-PLGA, FITC-labeled PEG-PLGA and glycidyl methacrylate derivatized dextran (Dex-GMA) are described in details in the supporting information section.

2. 3. Preparation and characterization of PLGA/PEG-PLGA NPs

2. 3. 1. Synthesis of PLGA/PEG-PLGA NPs

Blank and lysozyme loaded NPs were synthesized according to the method described by Haji Mansor et al., with some modifications [44]. Before being encapsulated in NPs, the lysozyme underwent nano-precipitation. Briefly, lysozyme dispersion at 2.0 % (w/v) and F-68 solution at 40 % (w/v) both in 0.15 M NaCl were mixed in a 1:1 volume ratio. Next, 25 µL of this protein solution was mixed with 975 µL of ice-cold glycofurol. After 10 minutes incubation on ice, the dispersion was gently vortexed and incubated again on ice for 20 minutes.

To synthesize the NPs, PLGA and PEG-PLGA were dissolved in DMI at a concentration of 12 % (w/v) at 40°C with continuous stirring. Subsequently, the two polymer solutions were combined in a glass vial at a volume ratio of 2:1 (PLGA:PEG-PLGA), yielding a total volume of 300 µL. To produce lysozyme loaded NPs, 100 µL of lysozyme precipitate in glycofurol were then introduced into the polymer mixture, while 100 µL of glycofurol were used for blank NPs. The resulting blend was subjected to high-speed stirring, and 200 µL of 0.05 M glycine-NaOH buffer at pH 11.4 was added to induce phase separation. After 1 minute, 500 µL of the same buffer was incrementally introduced every 30 seconds until reaching a total volume of 2.6 mL. To facilitate the removal of residual solvent from the NPs, the suspension was diluted with ultrapure water to a final volume of 30 mL. Following a 1-hour incubation at room temperature, the suspension was centrifuged at x 8500g for 30 minutes. The supernatant was discarded, and the pellet was suspended in 500 µL water. The NPs were consistently prepared fresh on the day of the experiment. The fluorescently labelled NPs were produced using exactly the same process, replacing 50% of the quantity of PEG-PLGA by FITC-PEG-PLGA.

2. 3. 2. Size distribution of NPs

The NP size distribution was determined by dynamic light scattering (DLS) on a Delsa NanoC instrument after dilution of the NPs dispersions in ultrapure water. The measurements were performed on 5 production batches, each measurement was performed in triplicate and a measure was the mean of 50 integration cycles.

2. 3. 3. Lysozyme encapsulation efficiency

Freeze-dried blank and lysozyme-loaded NPs were separately dissolved at 2.0 % (w:v) in DMSO at room temperature for 1 hour. The NPs were then disrupted by adding 0.01 M HCl in a 3:1 volume ratio. The solution was left to stand at room temperature for 1 hour and then diluted with 0.05 M Tris-HCl buffer pH 7.4 to perform the lysozyme assay as described in section 2. 7. Each measurement was performed in triplicate on three different NP production batches. The encapsulation efficiency, calculated as the ratio between the mass of bioactive lysozyme recovered from dissolve NPs and the initial mass of bioactive lysozyme, was about 44%.

2. 4. Synthesis and characterization of PolyHIPEs

2. 4. 1. PolyHIPE synthesis

In a standard procedure, Dex-GMA and F-68 were dissolved in an aqueous NP dispersion to produce an external phase containing 20 % (w:v) Dex-GMA, 2 % (w:v) F-68, and 2 % (w:v) NPs. For each polyHIPE, 400 µL of this external phase was introduced into a 5 ml glass vial and 50 µL of 8.0 % (w:w) LAP in ultrapure water was introduced and rapidly vortexed. Under constant vortex, dodecane (1.6 mL) was added dropwise to the aqueous phase. After complete addition of the oil phase, the mixture was further stirred by vortex for thirty seconds. The O/W HIPE was then placed under argon for another thirty seconds before light irradiation at 365 nm

for 25 min. The resulting polyHIPE was recovered and subjected to sequential washing steps: 100 % ethanol for 24 h, a mixture of 50 % PBS buffer and 50 % ethanol for 3 h, and finally, 100 % PBS buffer for an additional 24 h. For the washing of polyHIPEs used in the release study the PBS buffer was replaced by 0.05 M Tris-HCl (pH 7.4) buffer supplemented with 0.15 M NaCl. PolyHIPEs used in the cytocompatibility study were stored in ethanol after the first 100% ethanol bath, cut into precise sections in ethanol, subsequently washed in mixture of 50 % sterile PBS buffer and 50 % ethanol for 1 hour, followed by a 2-hour wash in sterile PBS buffer alone, before use.

Several formulations were used depending on the experimental requirements, introducing or not NPs and F-68, using lysozyme-loaded NPs or blank NPs, using FITC-labelled NPs and introducing unencapsulated lysozyme. Table S1 summarized all the formulations presented in this paper. When used, the unencapsulated lysozyme was introduced into the aqueous phase at a concentration of 6.9 µg/mL, mimicking the one encountered in loaded NPs.

2. 4. 2. PolyHIPE characterization

SEM images of the freeze dried polyHIPEs were collected with a Quanta 600 apparatus after metallization of the samples with gold (with Balzers SCD 004 Sputter Coater (BAL-TEC), vacuum of 5.10^{-2} Pa, current of 30 mA during 40 s). Pore and interconnection sizes were measured using the Image J software [46]. Mechanical compression tests were performed on polyHIPEs using a Zwick Roell Z050-2.5 kN cell instrument at a strain rate of 1 %.min^{-1}. The elastic modulus was determined by plotting the measured normal force between 0 % and 10 % strain and dividing the slope of the linear regression by the cross-sectional surface of the material. Confocal scanning light microscopy (CSLM) analysis was performed using a LSM 880 instrument (Zeiss, Germany) on fresh polyHIPEs. The latter were placed in a petri dish

with a coverslip base so that the material could be immersed in the buffer to prevent drying. Samples were observed in confocal mode with a 488 nm laser. Emitted light was recovered from 400 nm to 700 nm.

2. 5. *In vitro* cytocompatibility test

To assess the cytocompatibility of our biomaterials, cell metabolic activity and DNA content were assessed on Human Bone Marrow Mesenchymal Stromal Cells (hBM-MSCs) at day 0, 3 and 7 using the cell counting kit (CCK-8) assay and the PicoGreen assay respectively. For amplification, hBM-MSCs were seeded in complete culture medium (DMEM supplemented with 10 % (v:v) fetal bovine serum and 1 % (v:v) Penicillin/streptomycin (10000 $U.mL^{-1}$)) at 10000 cells/cm^2 in 75-cm^2 culture flasks, and medium was changed every other day. For cell experiments, hBM-MSCs were used at passage 4 and seeded at 10^4 cells/cm^2 in 24-well plates. Following cell adhesion (4 hours after seeding), quarter discs (3 mm thick and 1 cm of diameter) of biomaterial were immersed into the culture medium of each well using Transwell® cell culture inserts. Empty inserts with complete culture medium or supplemented with dimethylsulfoxide (DMSO) were used respectively as positive and negative control. Each condition was studied in triplicate at each time point, thereby ensuring the study of biomaterial pieces from distinct samples.

On designated culture days, cell metabolic activity was assessed using a CCK-8 solution (Sigma-Aldrich) per the supplier's recommendations. The absorbance of cell supernatants at 460 nm was measured (PowerWave X spectrophotometer, BioTek Intruments), and the results were normalized to absorbance of the positive control at D+1.

Regarding the measurement of DNA content, on designated culture days, cells were rinsed with PBS, and 500 µL of Tris/EDTA buffer was added before storing the plate at -80 °C for at least

24 hours. DNA content in each well was determined using a Quant-iT™ PicoGreen™ kit (Thermo Fisher Scientific) per manufacturer's recommendation.

2. 6. *In vitro* lysozyme release

Lysozyme release was investigated from both NPs and polyHIPEs and the lysozyme content in the release media was measured at various time intervals over 13 days. Both lysozyme-loaded NPs and blank NPs were tested. To assess the impact of lysozyme encapsulation in NP on the release kinetics, three polyHIPE formulations were evaluated: i) a polyHIPE containing blank NPs (PH_{NP+S}), ii) a polyHIPE containing blank NPs and unencapsulated lysozyme ($PH_{NP+S+Lyso}$) and iii) a polyHIPE containing lysozyme-loaded NPs (PH_{NP_lyso+S}). All experiments were conducted in triplicate.

Either 0.2 mL of NP dispersion or an entire polyHIPE was suspended in 5 mL of the release medium, consisting in 0.05 M Tris-HCl buffer pH 7.4, supplemented with 0.15 M NaCl and 1 $mg.mL^{-1}$ bovine serum albumin. The tubes were incubated at 37 °C with gentle agitation. At each designated time point, 1.5 mL of the buffer solution was collected and replaced with fresh buffer. For the NP samples, a prior centrifugation step (x 8500g for 30 minutes) was performed. The collected media were stored at -20°C for subsequent analysis.

2. 7. Bioactive lysozyme quantification

The quantity of bioactive lysozyme was estimated via the measurement of its biological activity as previously described with some modifications [47,48]. The enzymatic activity of lysozyme was determined by the measurement of the turbidity change in a Micrococcus lysodeikticus (ML) bacterial cell suspension. Briefly, a suspension of ML at 0.2 $g.L^{-1}$ was prepared in 0.05 M Tris-HCl (pH 7.4) under stirring at 37 °C for 1 hour. Then, 100 µL of samples was added to

2.9 mL of ML suspension and left to stir at 37 °C for 4 hours. Dilution were performed if needed and the absorbance at 450 nm was measured in microplates. The quantity of bioactive lysozyme was determined using a standard curve prepared from lysozyme dispersion ranging from 0 to 1000 $ng.mL^{-1}$.

2. 8. Statistical Analysis

Statistical analysis was performed using a two-way analysis of variance (ANOVA) to evaluate the effects of the experimental conditions. Three independent replicates were conducted for each condition (N=3). Post-hoc analysis was not performed as no significant interaction between factors was observed. Data are presented as mean ± standard deviation, and a p-value of less than 0.05 was considered statistically significant. All analyses were carried out using GraphPad Prism 9.5.1 software, and the assumptions of normality and homogeneity of variances were confirmed prior to ANOVA testing.

3. Results and discussion

3.1. Preparation of polymer precursors and NPs.

Dextran was chosen as polymer precursor for the preparation of the TE scaffolds because of its numerous advantages such as biocompatibility, biodegradability, and easy chemical modification notably to tailor mechanical strength and surface properties [49–51]. In the view of its structuration into macroporous materials through emulsion-templated radical polymerization, dextran was functionalized with methacrylate groups by reaction with glycidyl methacrylate following a method inspired by van Dijk-Wotthuis et al. [52]. Analysis by ^{1}H NMR confirmed the structure of the targeted Dex-GMA and revealed a functionalization degree of 47% (Figure S1) .

The NPs, intended to serve both as emulsion stabilizers and nanocarriers, were prepared from PLGA and PEG-PLGA. These polymers were synthetized by ring opening copolymerization of D,L-lactide and glycolide ([lactide]/[glycolide] = 75/25) using benzyl alcohol and monomethoxy-PEG_{5K} as initiator, respectively. The composition and molar mass of PLGA and of PEG-PLGA were determined by ^{1}H NMR based on the relative intensity of signals of the comonomers and of the initiators, namely $PLGA_{4.8\ K}$ and $PEG_{4.9K}$-*b*-$PLGA_{20.8K}$ with a lactide/glycolide molar ratio of 3/1 (Figure S2). The blank NPs synthesized from these polymers were characterized by an average diameter of 301 ± 36 nm according to DLS analysis (Figure S3).

To facilitate the detection and localization of the NPs within the scaffold, FITC-labeled NPs were also produced. For this purpose, the terminal hydroxy group of the PEG-PLGA was functionalized with FITC. The effective labeling of PEG-PLGA was proved by the detection of a UV signal in size exclusion chromatography (SEC) analysis of the treated copolymer PEG-PLGA-FITC, contrasting with the absence of any UV response for the pristine PEG-PLGA (Figure S4). Substituting part of the PEG-PLGA with FITC-labeled PEG-PLGA in the NP formulation has no significant impact on particle size (Figure S3).

3.2. Scaffold synthesis

The design of dextran-based scaffolds was then explored through high internal phase emulsion templating radical polymerization of Dex-GMA. Owing to the hydrosolubility of the methacrylate-functionalized dextran, oil-in-water (O/W) HIPEs were considered in order to locate the polymer precursor in the external aqueous phase of the emulsion before curing. As depicted in Figure 2, an O/W volume ratio of 80/20 was used, in line with the definition of

HIPE in which the internal phase must exceed 74% of the whole emulsion volume. The NPs were used as potential stabilizers of the HIPE. Given that the use of co-stabilizer in conjunction with particles is recognized to potentially enhance the interconnection of polyHIPEs prepared via Pickering emulsion [53–55], the addition of an amphiphilic PEO-PPO-PEO copolymer, namely F-68 (2 % (w:v)of the aqueous phase), in the HIPE formulation was tested (Table 1, entry 3). In order to evaluate the impact of NPs and F-68 on HIPE stabilization and polyHIPE structure, a HIPE was also formulated without stabilizer (Table 1, entry 1). In all cases, the HIPE curing process was achieved through light irradiation at 365 nm using LAP as photoinitiator (Figure 2). The latter was chosen for its non-toxicity and current use in biomedical applications.

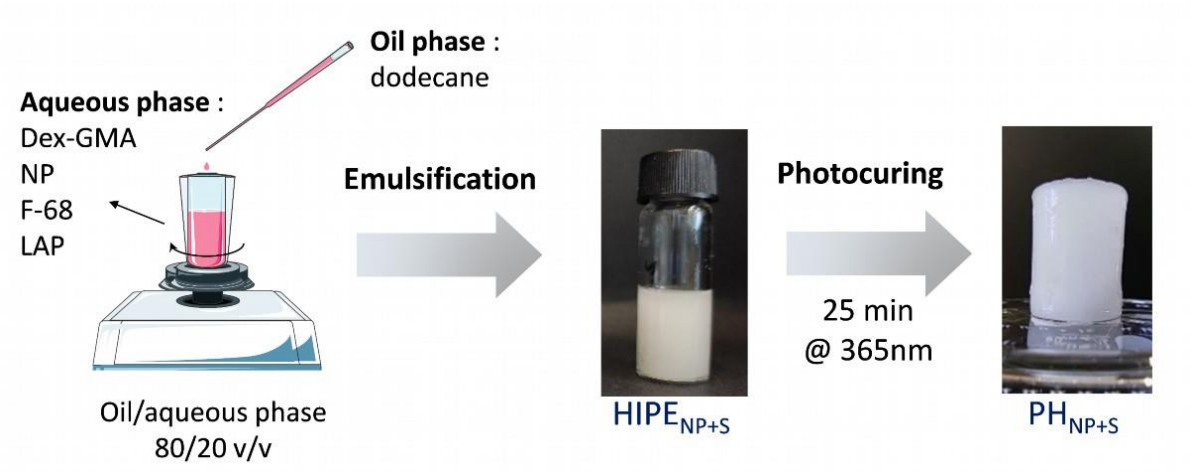

Figure 2. Emulsification process and HIPE photocuring leading to the corresponding PH_{NP+S} scaffold.

Table 1. Dextran-based polyHIPEs.

Entry	Samples	Dex-GMA (mg/mL)[a]	F-68 (mg/mL)[a]	NP (mg/mL)[a]	HIPE stability[b]	E (kPa)[c]
1	**PH_C**	200	0	0	±	31.29 ± 5.12
2	**PH_{NP}**	200	0	20	+	40.86 ± 1.56
3	**PH_{NP+S}**	200	20	20	+	83.48 ± 3.06

Conditions: oil phase = dodecane, $V_{oil\ phase}/V_{aqueous\ phase}$ = 80/20, LAP photoinitiator (10 mg/mL in the aqueous phase), photocuring for 25 min at 365 nm.[a] Concentrations of compounds in the aqueous phase. [b] + designates stable HIPE whereas ± indicates some variability in the emulsion stability. [c] Young Modulus measured by compression tests.

Regarding the HIPE formulation without any stabilizer (Table 1, entry 1), not all attempts were successful, stable HIPEs being obtained only occasionally, as illustrated in Figure S5. Nonetheless, when stable, this stabilizer-free emulsion was converted into a monolith (**PH_C**) through photocuring. Addition of PLGA/PEG-PLGA NPs to the emulsion formulation markedly improved the stability of the emulsion (Table 1, entry 2). In the latter case, stable HIPEs could consistently be produced and transformed into the corresponding monolith (**PH_{NP}**). This emphasized the emulsion stabilizing capacity of the NPs (Figure S5). As shown in Figure 2, HIPE formulation co-stabilized by NPs and F-68 (Table 1, entry 3) also led to stable emulsions and polyHIPE (**PH_{NP+S}**).

3.3. Scaffold morphology

SEM images evidenced that PH_C, PH_{NP} and PH_{NP+S} feature an open-cell porous structure characteristic of polyHIPEs with cavities interconnected by pores (Figure 3). Closer examination of the images indicates that PH_C and PH_{NP} have quite similar cavity size (around 60-70 µm). The degree of openness is lower in the case of PH_C and PH_{NP} as compared to the PH_{NP+S}. The limited degree of openness of the samples produced by the surfactant-free

procedures is consistent with the well-known role of the surfactant in the creation of interconnections [5,56] and the reinforcement of the film between the emulsion droplets by the NPs located at the interface [53,55,57]. The higher degree of openness led by the co-stabilization of the HIPE by NPs and F-68 is expected to favor cell penetration and proliferation. In this case, the average diameter of cavities is 46.9 µm and the pore diameters range from 1 to 35 µm, which is suitable for cell penetration in the scaffold.

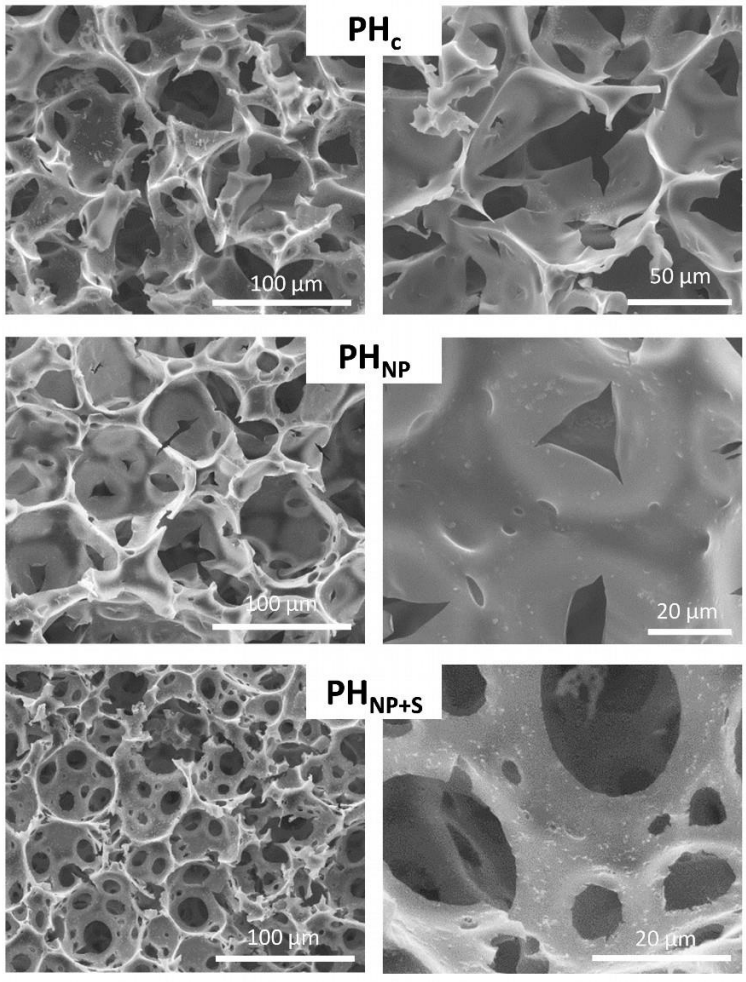

Figure 3. SEM micrographs of polyHIPEs PH_C, PH_{NP} and PH_{NP+S} produced from HIPEs without stabilizer, stabilized by NPs and co-stabilized by NPs and F-68, respectively.

To demonstrate the presence of the NPs in the final scaffolds, confocal laser scanning microscopy (CLSM) analyses were conducted on polyHIPEs formulated with FITC-labeled NPs in combination or not with F-68 (PH_{NP_FITC} and PH_{NP_FITC+S}) (Figure 4). The green coloration on the CLMS images confirms the presence of NPs embedded in the membranes of the polyHIPE, even after the washing steps. As negative control, dark CLMS images were recorded for the unlabeled PH_{NP+S}. While no specific accumulation of the NPs appears at the surface of the wall of PH_{NP_FITC+S}, the NPs were effectively integrated into the porous structure, where they are expected to fulfill their role of nanocarriers. As demonstrated by the comparison of images of PH_{NP_FITC} and PH_{NP_FITC+S}, the presence of the surfactant does not appear to affect the distribution of NPs in polymer the matrix.

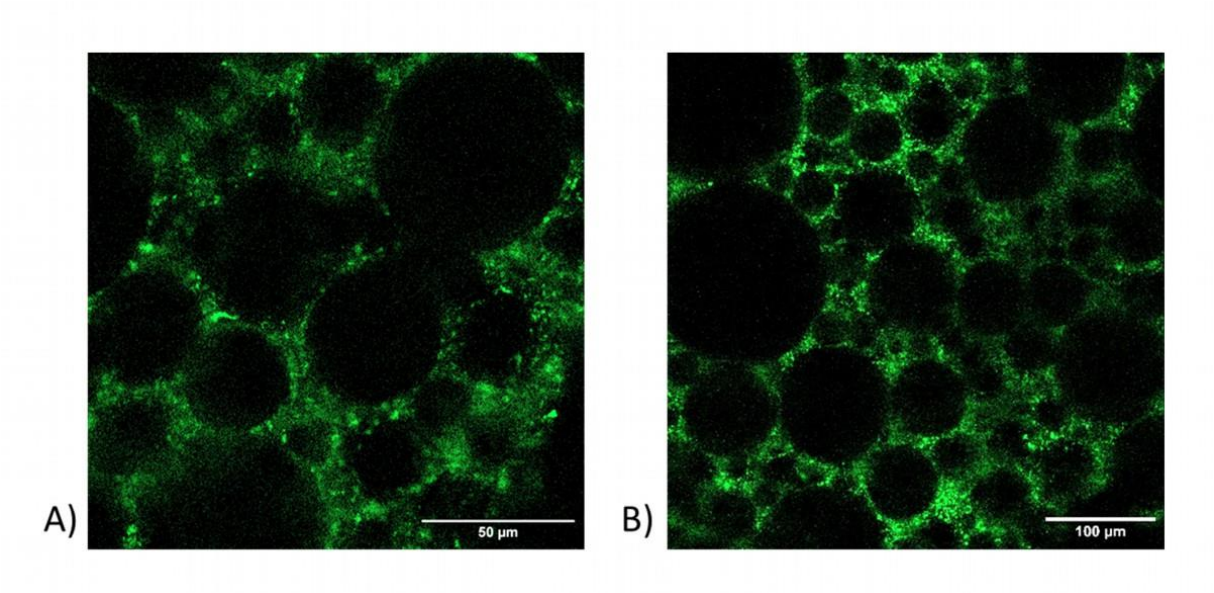

Figure 4. CLSM micrographs of PH_{NP_FITC} (A) and PH_{NP_FITC+S} (B) containing NPs formulated with FITC-labeled PEG-PLGA.

3.4. Mechanical properties

The mechanical properties of scaffolds are crucial as they need to closely match those of the targeted tissues. These properties also exert a significant influence on cell behavior, as cells can exhibit different phenotypes based on their environment [58]. Hence, compressive stress measurements were conducted on the different polyHIPEs, as depicted in Figure 5. The Young's moduli are given in Table 1. The Young's modulus of PH_{NP} (41 kPa) was slightly higher than the one of PH_c (31 kPa) probably due to the reinforcement of the dextran matrix by the embedded NPs. Furthermore, the introduction of the F-68 co-stabilizer almost doubles the Young's modulus of the scaffold, with PH_{NP+S} exhibiting a modulus of 83 kPa. In addition to the potential reinforcement of the matrix by the co-stabilizer, this enhancement in mechanical properties could also be attributed in part to the reduction in cavity size within the material. Overall, these scaffolds exhibited compressive Young's moduli ranging from low to moderate levels. This characteristic makes them particularly suitable for tissue regeneration applications in organs with inherently low stiffness, such as muscles (5-170 kPa) , skin (35-850 kPa) and spleen (~ 20 kPa), to name a few [59].

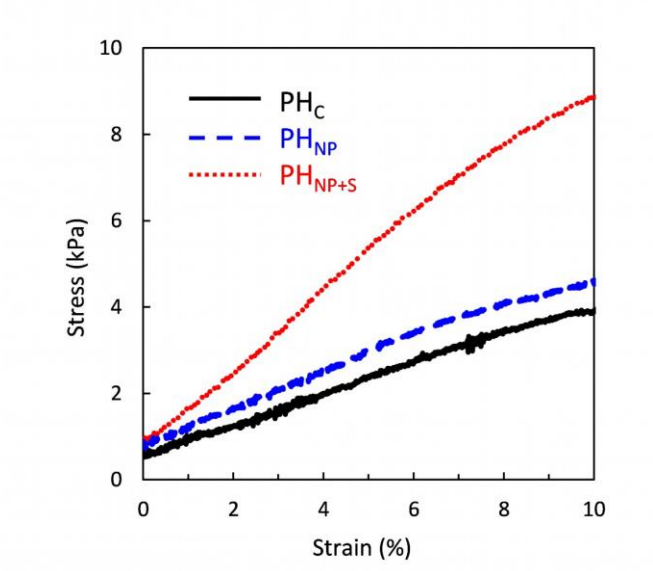

Figure 5. Compressive stress-strain curves for PH_C (black line), PH_{NP} (blue line) and PH_{NP+S} (red line) measured at a strain rate of 1 %.min^{-1}.

This is the author's version of the article published in Colloids and Surfaces B: Biointerfaces. Changes were made to this version by the publisher prior to publication. The final version is available at 10.1016/j.colsurfb.2024.114342

3.5. Cytotoxicity

The potential cytotoxicity of our polyHIPE formulations has been evaluated using the CCK-8 assay based on the dehydrogenase activity detection of viable cells and total dsDNA content measured by the Picogreen dye. First, as shown in Figure 6, dsDNA content measurement indicates a significant increase from day 1 to day 3 ($p \leq 0.05$) in all tested conditions and in a comparative manner. This observation suggests that our biomaterials do not have a negative effect on cell proliferation and number after 3 days of culture. Furthermore, from day 3 to day 7, dsDNA content does not increase in all conditions indicating an absence of cell number increase. It is noteworthy that this observation is associated with a significant decrease of the metabolic activity from day 3 to 7. Consequently, in all conditions, the measured stable cell number (from day 3 to day 7) can be attributed to a decrease in cell proliferation which is expected given that hBM-MSC confluence is reached after day 5 in our cell culture conditions. Collectively, these results indicate that our polyHIPE formulations do not exert an indirect effect on hBM-MSCs viability and proliferation.

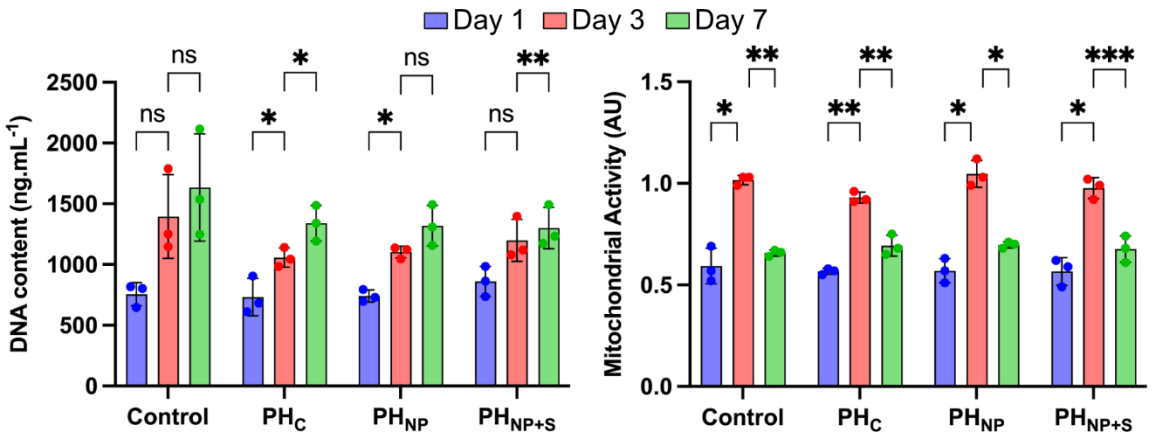

Figure 6. DNA content and mitochondrial activity measured on hBM-MSCs cultured without polyHIPE (control) or in indirect contact with PH_C, PH_{NP} or $PH_{NP\text{-}S}$. N=3 for each formulation. Analysis of variance test (ANOVA) : ns for $p > 0.05$, * for $p \leq 0.05$, ** for $p \leq 0.01$ and *** for $p \leq 0.001$.

3.6. Model protein release

The release of lysozyme from (i) the lysozyme-loaded NPs, (ii) the polyHIPEs loaded with free lysozyme molecules and (iii) the lysozyme-loaded NPs incorporated into a polyHIPE is shown in Figure 7. Around 40% of the encapsulated lysozyme is released from the NPs after just a few hours. This initial burst effect is consistent with previous results obtained on similar NPs [44]. This may reflect the rapid release of bioactive proteins that have been brought close to the NP surface by the efflux of residual solvents during the purification step. After this increase, the release speed decreases but continues steadily for 6 days suggesting the diffusion of proteins from deeper parts of the NPs. The release reaches a plateau after 6 days with almost 80% of the loaded bioactive lysozyme released. The biphasic release patterns observed in lysozyme is also consistent with literature data on PEG-containing PLGA NPs [60]. Indeed, at pH 7.4, these NPs are expected to establish electrostatic interactions with the positively-charged lysozyme molecules (pI = 11.35), which hinders their release. These interactions seem to be the major factor for protein load entrapment, as no further protein release was observed despite the continuous degradation of PLGA matrices into acidic reactant.

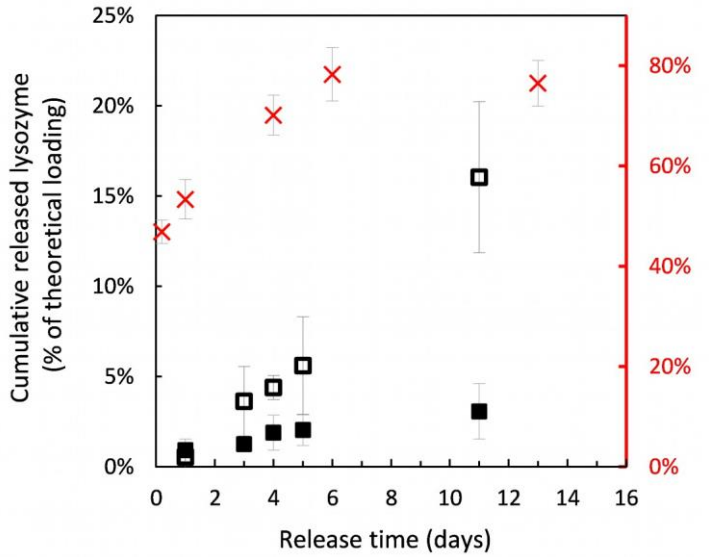

Figure 7. Cumulative release of lysozyme in 0.05 M Tris-HCl buffer pH 7.4 from (i) NPs (red crosses, right axis), from (ii) polyHIPEs containing blank NPs and free lysozyme (empty squares, left axis) and from (iii) polyHIPEs containing lysozyme-loaded NPs (solid squares, left axis). N=3 for each formulation.

When dispersed in the matrix of the polyHIPEs stabilized by blank NPs (Figure 7 (ii)), the lysozyme is released continuously with no burst effect and 16% of bioactive lysozyme is released after 11 days with disappearance of the plateau observed in case (i). The slower release compared to NPs alone is easily explained by the physical barrier formed by the crosslinked dextran matrix which may slow down the diffusion of the protein and further delay the release of lysozyme from the scaffold. As a result, the amount of total released protein and the time required to reach the interconnected internal macroporous cavities of the polyHIPEs are reduced and delayed. Similarly, lysozyme release from the polyHIPEs stabilized by loaded NP (case iii) is gradual up to day 11 but only reaches a total release of 3 % of the bioactive lysozyme. The

encapsulation of the protein in NPs has been demonstrated to maintain its bioactivity, and polyHIPEs formulated with unprotected free protein show an intermediate release rate. The lower release rate in case iii) as compared to the two other samples can be explained by the double physical barrier exerted by the NP core on the one hand, and by the polymeric dextran network on the other, drastically reducing the rate of protein release into the external medium.

The current concept of encapsulating the active protein within NPs prior their loading in the porous scaffolds is innovative and provides additional control on their release rate. Indeed, numerous polyHIPEs produced by Pickering emulsion [35–38] were previously investigated as supports for tissue engineering including bioactive PCL- and PLGA-based scaffolds but, in these cases, the API, such as anti-inflammatory drugs, were incorporated directly in the polymer matrix and not in the particles [39–41]. Interestingly, by preserving the encapsulated protein bioactivity and allowing a slow release rate, our proposed strategy notably paves the way towards the development of materials that facilitate the cell-dependent release of bioactive molecules. Moreover, different therapeutic proteins could be combined in the matrix and the core of the NPs in order to adjust the short and long term release profiles of the latter to address the specific demand of specific tissue engineering applications. However, while this approach enhances control, the steps involved in protein encapsulation in NPs may introduce an additional level of complexity in the manufacturing process, hence potentially affecting scalability. Nonetheless, the encapsulation of proteins in NPs embedded in porous polymer matrices also represents a valuable lever to tailor release profiles to specific needs beyond the regenerative medicine area. For example, the porous materials developed in this work could be applied to *in vitro* 2D or 3D cell models, such as spheroids and organoids, as polyHIPEs have shown suitable interconnected porosity to support the formation of three-dimensional neural cell networks for brain tissue regeneration [61]. Our composite polyHIPEs could also be

explored for therapeutic applications in oncology, particularly in strategies targeting solid tumors including tumor cell trapping [62], immunostimulation, drug delivery and cell differentiation [63]. As an example, bio-interactive implants for the treatment of glioblastoma [42], an aggressive primary brain cancer, have been already evaluated in *vitro*, ex *vivo*, and on animal models. They include fibrous composite chitosan nanofibers embedding loaded NPs [64], silk fibroin sponges loaded with therapeutic protein [65] and injectable hydrogels [66]. This therapeutic approach implies to control key features in terms of cancer cell migration, differentiation and sensitivity to elimination signals but also porosity and stiffness of the bioimplants as well as controlled release performances of APIs. In the light of these considerations, our interconnected porous polyHIPE scaffolds combined with APIs loaded NPs appear as good candidates for natural cell migration, and would offer the ability to control the macro-arrangement of cells into structures that are not limited by diffusion of API, nutrients and waste. Such new biomaterials should be evaluated in the future in both *in vitro* and *in vivo* models to demonstrate their interest in soft tissue engineering and cancer therapy.

4. Conclusion

Innovative 3D-interconnected dextran-based scaffolds loaded with PLGA/PEG-PLGA NPs were fabricated via a straightforward emulsion templating polymerization method. In this case, NPs served as both stabilizers of the emulsion template and potential nanocarriers of active pharmaceutical ingredients, including proteins, notably to promote cell growth and proliferation. Although stable HIPEs and the corresponding porous polyHIPE structures were achieved using NPs as sole stabilizer, the addition of a co-stabilizer improved the interconnectivity of the scaffold. The resulting NPs-loaded scaffolds showed low Young's moduli matching those of soft tissues like kidney, brain, or liver. In all the cases, excellent cell

viability was recorded confirming that the scaffolds do not exert an indirect effect on hBM-MSCs viability and proliferation. Finally, lysozyme served as model protein and was encapsulated in the NPs and/or loaded in the scaffolds. Scaffolds loaded with free lysozyme offered a slower and more continuous release of the bioactive protein compared to the lysozyme loaded NPs. Moreover, embedding the lysozyme-loaded NPs within the dextran-based scaffold further slowed down the release of the protein, as this requires the lysozyme to exit the NPs core and pass through the crosslinked dextran matrix. Compared to earlier systems where protein or API was directly loaded into porous matrices, encapsulating protein in NPs within scaffolds preserves protein integrity and offers greater control over release. This concept presents numerous opportunities for fine-tuning both short- and long-term release profiles to meet the requirements of specific regenerative medicine applications.

Acknowledgment

This work was funded by the Institut National de la Santé et de la Recherche Médicale (INSERM) the University of Nantes, and the University of Angers. M.D obtained a postdoctoral fellowship from « Région Pays de la Loire » through Bioactive Scaffolds from Pickering Emulsions for Enhanced Bone Osteogenesis « Speebo » project, part of the Bioregate program. A.D. is FNRS Senior Research Associate and thanks the F.R.S.-FNRS for financial support. The authors acknowledge the SC3M plateform from the Inserm/NU/ONIRIS UMR1229 RMeS Laboratory and SFR François Bonamy-UMS 016, as well as the GIGA Cell Imaging core facility. F.B. also thanks the French National Agency for Research (ANR) under the frame of EuroNanoMed III (project GLIOSILK) [ANR-19-ENM3-0003-01] (FB as a member of the funded team) and the "Comité Départemental de Maine-et-Loire de la Ligue contre le Cancer"

(CD49) under the frame of the FusTarG project (FB as a member of the funded team). The program VINCI 2020—Université Franco Italienne (project number: C3-1419, "Novel nanotechnological approaches for glioblastoma targeting" attributed to FB) also supported this research through a PhD fellowship to AR. The authors are also grateful to Dr. Virginie Bertrand from ULiege for skillful assistance with cell culture tests, to Grégory Cartigny, Valérie Collard and Martine Dejeneffe from ULiege for their regular help with polymer synthesis, NMR and microscopy analyses.

References.

[1] B. Aldemir Dikici, F. Claeyssens, Basic Principles of Emulsion Templating and Its Use as an Emerging Manufacturing Method of Tissue Engineering Scaffolds, Front Bioeng Biotechnol 8 (2020). https://doi.org/10.3389/fbioe.2020.00875.

[2] S. Kramer, N.R. Cameron, P. Krajnc, Porous polymers from high internal phase emulsions as scaffolds for biological applications, Polymers (Basel) 13 (2021) 1–24. https://doi.org/10.3390/polym13111786.

[3] R. Foudazi, HIPEs to PolyHIPEs, React Funct Polym 164 (2021) 104917. https://doi.org/10.1016/j.reactfunctpolym.2021.104917.

[4] J. Luo, Z. Huang, L. Liu, H. Wang, G. Ruan, C. Zhao, F. Du, Recent advances in separation applications of polymerized high internal phase emulsions, J Sep Sci 44 (2021) 169–187. https://doi.org/10.1002/jssc.202000612.

[5] T. Zhang, R.A. Sanguramath, S. Israel, M.S. Silverstein, Emulsion Templating: Porous Polymers and Beyond, Macromolecules 52 (2019) 5445–5479. https://doi.org/10.1021/acs.macromol.8b02576.

[6] A.C. Nalawade, R. V. Ghorpade, S. Shadbar, M.S. Qureshi, N.N. Chavan, A.A. Khan, S. Ponrathnam, Inverse high internal phase emulsion polymerization (i-HIPE) of GMMA, HEMA and GDMA for the preparation of superporous hydrogels as a tissue

engineering scaffold, J Mater Chem B 4 (2016) 450–460. https://doi.org/10.1039/c5tb01873k.

[7] A.M. Eissa, F.S.V. Barros, P. Vrljicak, J.J. Brosens, N.R. Cameron, Enhanced Differentiation Potential of Primary Human Endometrial Cells Cultured on 3D Scaffolds, Biomacromolecules 19 (2018) 3343–3350. https://doi.org/10.1021/acs.biomac.8b00635.

[8] M.E. Whitely, J.L. Robinson, M.C. Stuebben, H.A. Pearce, M.A.P. McEnery, E. Cosgriff-Hernandez, Prevention of Oxygen Inhibition of PolyHIPE Radical Polymerization Using a Thiol-Based Cross-Linker, ACS Biomater Sci Eng 3 (2017) 409–419. https://doi.org/10.1021/acsbiomaterials.6b00663.

[9] R.S. Moglia, J.L. Holm, N.A. Sears, C.J. Wilson, D.M. Harrison, E. Cosgriff-Hernandez, Injectable polyHIPEs as high-porosity bone grafts, Biomacromolecules 12 (2011) 3621–3628. https://doi.org/10.1021/bm2008839.

[10] A.R. Murphy, I. Ghobrial, P. Jamshidi, A. Laslett, C.M. O'Brien, N.R. Cameron, Tailored emulsion-templated porous polymer scaffolds for iPSC-derived human neural precursor cell culture, Polym Chem 8 (2017) 6617–6627. https://doi.org/10.1039/c7py01375b.

[11] A.R. Murphy, J.M. Haynes, A.L. Laslett, N.R. Cameron, C.M. O'Brien, Three-dimensional differentiation of human pluripotent stem cell-derived neural precursor cells using tailored porous polymer scaffolds, Acta Biomater 101 (2020) 102–116. https://doi.org/10.1016/j.actbio.2019.10.017.

[12] B. Aldemir Dikici, G.C. Reilly, F. Claeyssens, Boosting the Osteogenic and Angiogenic Performance of Multiscale Porous Polycaprolactone Scaffolds by in Vitro Generated Extracellular Matrix Decoration, ACS Appl Mater Interfaces 12 (2020) 12510–12524. https://doi.org/10.1021/acsami.9b23100.

[13] B. Aldemir Dikici, C. Sherborne, G.C. Reilly, F. Claeyssens, Emulsion templated scaffolds manufactured from photocurable polycaprolactone, Polymer (Guildf) 175 (2019) 243–254. https://doi.org/10.1016/j.polymer.2019.05.023.

[14] K. Kapilov-Buchman, T. Bialystocki, D. Niezni, L. Perry, S. Levenberg, M.S. Silverstein, Porous polycaprolactone and polycarbonate poly(urethane urea)s via

emulsion templating: Structures, properties, cell growth, Polym Chem (2021) 6569–6581. https://doi.org/10.1039/d1py01106e.

[15] K. Kapilov-Buchman, T. Bialystocki, D. Niezni, L. Perry, S. Levenberg, M.S. Silverstein, Porous polycaprolactone and polycarbonate poly(urethane urea)s via emulsion templating: Structures, properties, cell growth, Polym Chem (2021) 6569–6581. https://doi.org/10.1039/d1py01106e.

[16] D. Diekjürgen, D.W. Grainger, Polysaccharide matrices used in 3D in vitro cell culture systems, Biomaterials 141 (2017) 96–115. https://doi.org/10.1016/j.biomaterials.2017.06.020.

[17] A. Barbetta, M. Massimi, B. Di Rosario, S. Nardecchia, M. De Colli, L.C. Devirgiliis, M. Dentini, Emulsion templated scaffolds that include gelatin and glycosaminoglycans, Biomacromolecules 9 (2008) 2844–2856. https://doi.org/10.1021/bm800599d.

[18] L. Avraham, R.A. Sanguramath, O. Cohen, L. Perry, S. Levenberg, M.S. Silverstein, Polysaccharide-based, emulsion-templated, porous poly(urethane urea)s: Composition, catalysis, cell growth, Eur Polym J 169 (2022) 111140. https://doi.org/10.1016/j.eurpolymj.2022.111140.

[19] A. Barbetta, M. Massimi, B. Di Rosario, S. Nardecchia, M. De Colli, L.C. Devirgiliis, M. Dentini, Emulsion templated scaffolds that include gelatin and glycosaminoglycans, Biomacromolecules 9 (2008) 2844–2856. https://doi.org/10.1021/bm800599d.

[20] A. Barbetta, M. Dentini, E.M. Zannoni, M.E. De Stefano, Tailoring the porosity and morphology of gelatin-methacrylate polyHIPE scaffolds for tissue engineering applications, Langmuir 21 (2005) 12333–12341. https://doi.org/10.1021/la0520233.

[21] O.C. Onder, P. Utroša, S. Caserman, M. Podobnik, M.T. Žnidarič, J. Grdadolnik, S. Kovačič, E. Žagar, D. Pahovnik, Emulsion-templated synthetic polypeptide scaffolds prepared by ring-opening polymerization of: N -carboxyanhydrides, Polym Chem 11 (2020) 4260–4270. https://doi.org/10.1039/d0py00387e.

[22] A. Rigg, P. Champagne, M.F. Cunningham, Polysaccharide-Based Nanoparticles as Pickering Emulsifiers in Emulsion Formulations and Heterogenous Polymerization

Systems, Macromol Rapid Commun 43 (2022) 1–29. https://doi.org/10.1002/marc.202100493.

[23] H. Dupont, V. Maingret, V. Schmitt, V. Héroguez, New Insights into the Formulation and Polymerization of Pickering Emulsions Stabilized by Natural Organic Particles, Macromolecules 54 (2021) 4945–4970. https://doi.org/10.1021/acs.macromol.1c00225.

[24] B. Pang, H. Liu, K. Zhang, Recent progress on Pickering emulsions stabilized by polysaccharides-based micro/nanoparticles, Adv Colloid Interface Sci 296 (2021) 102522. https://doi.org/10.1016/j.cis.2021.102522.

[25] T. Zhang, F. Liu, J. Wu, T. Ngai, Pickering emulsions stabilized by biocompatible particles: A review of preparation, bioapplication, and perspective, Particuology 64 (2022) 110–120. https://doi.org/10.1016/j.partic.2021.07.003.

[26] B. Robin, C. Albert, M. Beladjine, F.X. Legrand, S. Geiger, L. Moine, V. Nicolas, A. Canette, M. Trichet, N. Tsapis, F. Agnely, N. Huang, Tuning morphology of Pickering emulsions stabilised by biodegradable PLGA nanoparticles: How PLGA characteristics influence emulsion properties, J Colloid Interface Sci 595 (2021) 202–211. https://doi.org/10.1016/j.jcis.2021.03.061.

[27] F. Qi, J. Wu, G. Sun, F. Nan, T. Ngai, G. Ma, Systematic studies of Pickering emulsions stabilized by uniform-sized PLGA particles: Preparation and stabilization mechanism, J Mater Chem B 2 (2014) 7605–7611. https://doi.org/10.1039/c4tb01165a.

[28] Abdullah, J. Weiss, T. Ahmad, C. Zhang, H. Zhang, A review of recent progress on high internal-phase Pickering emulsions in food science, Trends Food Sci Technol 106 (2020) 91–103. https://doi.org/10.1016/j.tifs.2020.10.016.

[29] Q. Zhao, F. Zaaboul, Y. Liu, J. Li, Recent advances on protein-based Pickering high internal phase emulsions (Pickering HIPEs): Fabrication, characterization, and applications, Compr Rev Food Sci Food Saf 19 (2020) 1934–1968. https://doi.org/10.1111/1541-4337.12570.

[30] E. Durgut, C. Sherborne, B. Aldemir Dikici, G.C. Reilly, F. Claeyssens, Preparation of Interconnected Pickering Polymerized High Internal Phase Emulsions by Arrested

Coalescence, Langmuir 38 (2022) 10953–10962. https://doi.org/10.1021/acs.langmuir.2c01243.

[31] I. Berezovska, K. Kapilov, P. Dhavalikar, E. Cosgriff-Hernandez, M.S. Silverstein, Reactive Surfactants for Achieving Open-Cell PolyHIPE Foams from Pickering Emulsions, Macromol Mater Eng 306 (2021) 1–8. https://doi.org/10.1002/mame.202000825.

[32] H. Dupont, C. Fouché, M.A. Dourges, V. Schmitt, V. Héroguez, Polymerization of cellulose nanocrystals-based Pickering HIPE towards green porous materials, Carbohydr Polym 243 (2020). https://doi.org/10.1016/j.carbpol.2020.116411.

[33] X. Yang, D. Qi, K. Xu, A. Alimu, L. Cao, Bio-compatible n-HAPs/polymer monolithic composites templated from CO2-in-water high internal phase emulsions, React Funct Polym 181 (2022) 105417. https://doi.org/10.1016/j.reactfunctpolym.2022.105417.

[34] H. Tan, J. Wei, G. Sun, C. Mu, W. Lin, T. Ngai, Interconnected macroporous 3D scaffolds templated from gelatin nanoparticle-stabilized high internal phase emulsions for biomedical applications, Soft Matter 13 (2017) 3871–3878. https://doi.org/10.1039/c7sm00706j.

[35] H. Tan, Z. Tu, H. Jia, X. Gou, T. Ngai, Hierarchical Porous Protein Scaffold Templated from High Internal Phase Emulsion Costabilized by Gelatin and Gelatin Nanoparticles, Langmuir 34 (2018) 4820–4829. https://doi.org/10.1021/acs.langmuir.7b04047.

[36] F. Kavousi, N. Nikfarjam, Highly interconnected macroporous structures made from starch nanoparticle-stabilized medium internal phase emulsion polymerization for use in cell culture, Polymer (Guildf) 180 (2019) 121744. https://doi.org/10.1016/j.polymer.2019.121744.

[37] T. Yang, Y. Hu, C. Wang, B.P. Binks, Fabrication of Hierarchical Macroporous Biocompatible Scaffolds by Combining Pickering High Internal Phase Emulsion Templates with Three-Dimensional Printing, ACS Appl Mater Interfaces 9 (2017) 22950–22958. https://doi.org/10.1021/acsami.7b05012.

[38] J. Wang, H. Gao, Y. Hu, N. Zhang, W. Zhou, C. Wang, B.P. Binks, Z. Yang, 3D printing of Pickering emulsion inks to construct poly(D,L-lactide-co-trimethylene carbonate)-

based porous bioactive scaffolds with shape memory effect, J Mater Sci 56 (2021) 731–745. https://doi.org/10.1007/s10853-020-05318-7.

[39] Y. Hu, X. Gu, Y. Yang, J. Huang, M. Hu, W. Chen, Z. Tong, C. Wang, Facile fabrication of poly(l -Lactic Acid)-Grafted hydroxyapatite/poly(lactic- co -glycolic Acid) scaffolds by pickering high internal phase emulsion templates, ACS Appl Mater Interfaces 6 (2014) 17166–17175. https://doi.org/10.1021/am504877h.

[40] Y. Hu, H. Gao, Z. Du, Y. Liu, Y. Yang, C. Wang, Pickering high internal phase emulsion-based hydroxyapatite-poly(ε-caprolactone) nanocomposite scaffolds, J Mater Chem B 3 (2015) 3848–3857. https://doi.org/10.1039/c5tb00093a.

[41] Y. Hu, J. Wang, X. Li, X. Hu, W. Zhou, X. Dong, C. Wang, Z. Yang, B.P. Binks, Facile preparation of bioactive nanoparticle/poly(ε-caprolactone) hierarchical porous scaffolds via 3D printing of high internal phase Pickering emulsions, J Colloid Interface Sci 545 (2019) 104–115. https://doi.org/10.1016/j.jcis.2019.03.024.

[42] M.H. Mansor, E. Garcion, B. Ramalapa, N. Buchtova, C. Toullec, M. Aucamp, J. Le Bideau, F. Hindré, A. Dube, C. Alvarez-Lorenzo, M. Galleni, C. Jérôme, F. Boury, Polymer-Based Protein Delivery Systems for Loco-Regional Administration, in: Green Synthesis in Nanomedicine and Human Health, CRC Press, First edition. | Boca Raton, FL : CRC Press, [2021], 2021: pp. 249–270. https://doi.org/10.1201/9781003023197-17.

[43] A. Swed, T. Cordonnier, A. Dénarnaud, C. Boyer, J. Guicheux, P. Weiss, F. Boury, Sustained release of TGF-β1 from biodegradable microparticles prepared by a new green process in CO2 medium, Int J Pharm 493 (2015) 357–365. https://doi.org/10.1016/j.ijpharm.2015.07.043.

[44] M. Haji Mansor, M. Najberg, A. Contini, C. Alvarez-Lorenzo, E. Garcion, C. Jérôme, F. Boury, Development of a non-toxic and non-denaturing formulation process for encapsulation of SDF-1α into PLGA/PEG-PLGA nanoparticles to achieve sustained release, European Journal of Pharmaceutics and Biopharmaceutics 125 (2018) 38–50. https://doi.org/10.1016/j.ejpb.2017.12.020.

[45] A.-L. Lainé, E. Adriaenssens, A. Vessières, G. Jaouen, C. Corbet, E. Desruelles, P. Pigeon, R.-A. Toillon, C. Passirani, The in vivo performance of ferrocenyl tamoxifen

lipid nanocapsules in xenografted triple negative breast cancer, Biomaterials 34 (2013) 6949–6956. https://doi.org/10.1016/j.biomaterials.2013.05.065.

[46] J. Schindelin, I. Arganda-Carreras, E. Frise, V. Kaynig, M. Longair, T. Pietzsch, S. Preibisch, C. Rueden, S. Saalfeld, B. Schmid, J.Y. Tinevez, D.J. White, V. Hartenstein, K. Eliceiri, P. Tomancak, A. Cardona, Fiji: An open-source platform for biological-image analysis, Nat Methods 9 (2012) 676–682. https://doi.org/10.1038/nmeth.2019.

[47] A. Aubert-Pouëssel, D.C. Bibby, M.C. Venier-Julienne, F. Hindré, J.P. Benoît, A novel in vitro delivery system for assessing the biological integrity of protein upon release from PLGA microspheres, Pharm Res 19 (2002) 1046–1051. https://doi.org/10.1023/A:1016482809810.

[48] H.A. McKenzie, F.H. White, Determination of lysozyme activity at low levels with emphasis on the milk enzyme, Anal Biochem 157 (1986) 367–374. https://doi.org/10.1016/0003-2697(86)90639-1.

[49] N. Ahmed Omar, J. Amédée, D. Letourneur, J.-C. Fricain, M. Fenelon, Recent Advances of Pullulan and/or Dextran-Based Materials for Bone Tissue Engineering Strategies in Preclinical Studies: A Systematic Review, Front Bioeng Biotechnol 10 (2022). https://doi.org/10.3389/fbioe.2022.889481.

[50] G. Sun, J.J. Mao, Engineering Dextran-Based Scaffolds for Drug Delivery and Tissue Repair, Nanomedicine 7 (2012) 1771–1784. https://doi.org/10.2217/nnm.12.149.

[51] Y. Zhao, S. Jalili, Dextran, as a biological macromolecule for the development of bioactive wound dressing materials: A review of recent progress and future perspectives, Int J Biol Macromol 207 (2022) 666–682. https://doi.org/10.1016/j.ijbiomac.2022.02.114.

[52] W.N.E. van Dijk-Wotthuis, O. Franssen, H. Talsma, M.J. van Steenbergen, J.J. Kettenes-van den Bosch, W.E. Hennink, Synthesis, Characterization, and Polymerization of Glycidyl Methacrylate Derivatized Dextran, Macromolecules 28 (1995) 6317–6322. https://doi.org/10.1021/ma00122a044.

[53] E. Durgut, C. Sherborne, B. Aldemir Dikici, G.C. Reilly, F. Claeyssens, Preparation of Interconnected Pickering Polymerized High Internal Phase Emulsions by Arrested

Coalescence, Langmuir 38 (2022) 10953–10962. https://doi.org/10.1021/acs.langmuir.2c01243.

[54] L.L.C. Wong, V.O. Ikem, A. Menner, A. Bismarck, Macroporous Polymers with Hierarchical Pore Structure from Emulsion Templates Stabilised by Both Particles and Surfactants a, (2011) 1563–1568. https://doi.org/10.1002/marc.201100382.

[55] A. Vílchez, C. Rodríguez-Abreu, A. Menner, A. Bismarck, J. Esquena, Antagonistic effects between magnetite nanoparticles and a hydrophobic surfactant in highly concentrated pickering emulsions, Langmuir 30 (2014) 5064–5074. https://doi.org/10.1021/la4034518.

[56] J.M. Williams, D.A. Wrobleski, Spatial distribution of the phases in water-in-oil emulsions. Open and closed microcellular foams from cross-linked polystyrene, Langmuir 4 (1988) 656–662. https://doi.org/10.1021/la00081a027.

[57] L.L.C. Wong, V.O. Ikem, A. Menner, A. Bismarck, Macroporous Polymers with Hierarchical Pore Structure from Emulsion Templates Stabilised by Both Particles and Surfactants a, (2011) 1563–1568. https://doi.org/10.1002/marc.201100382.

[58] Z. Terzopoulou, A. Zamboulis, I. Koumentakou, G. Michailidou, M.J. Noordam, D.N. Bikiaris, Biocompatible Synthetic Polymers for Tissue Engineering Purposes, Biomacromolecules 23 (2022) 1841–1863. https://doi.org/10.1021/acs.biomac.2c00047.

[59] C.F. Guimarães, L. Gasperini, A.P. Marques, R.L. Reis, The stiffness of living tissues and its implications for tissue engineering, Nat Rev Mater 5 (2020) 351–370. https://doi.org/10.1038/s41578-019-0169-1.

[60] M.J. Santander-Ortega, N. Csaba, L. González, D. Bastos-González, J.L. Ortega-Vinuesa, M.J. Alonso, Protein-loaded PLGA–PEO blend nanoparticles: encapsulation, release and degradation characteristics, Colloid Polym Sci 288 (2010) 141–150. https://doi.org/10.1007/s00396-009-2131-z.

[61] A.R. Murphy, J.M. Haynes, A.L. Laslett, N.R. Cameron, C.M. O'Brien, Three-dimensional differentiation of human pluripotent stem cell-derived neural precursor cells using tailored porous polymer scaffolds, Acta Biomater 101 (2020) 102–116. https://doi.org/10.1016/j.actbio.2019.10.017.

[62] M. Najberg, M. Haji Mansor, F. Boury, C. Alvarez-Lorenzo, E. Garcion, Reversing the Tumor Target: Establishment of a Tumor Trap, Front Pharmacol 10 (2019). https://doi.org/10.3389/fphar.2019.00887.

[63] R. Molina-Peña, N.H. Ferreira, C. Roy, L. Roncali, M. Najberg, S. Avril, M. Zarur, W. Bourgeois, A. Ferreirós, C. Lucchi, F. Cavallieri, F. Hindré, G. Tosi, G. Biagini, F. Valzania, F. Berger, M. Abal, A. Rousseau, F. Boury, C. Alvarez-Lorenzo, E. Garcion, Implantable SDF-1α-loaded silk fibroin hyaluronic acid aerogel sponges as an instructive component of the glioblastoma ecosystem: Between chemoattraction and tumor shaping into resection cavities, Acta Biomater 173 (2024) 261–282. https://doi.org/10.1016/j.actbio.2023.10.022.

[64] R. Molina-Peña, M. Haji Mansor, M. Najberg, J.-M. Thomassin, B. Gueza, C. Alvarez-Lorenzo, E. Garcion, C. Jérôme, F. Boury, Nanoparticle-containing electrospun nanofibrous scaffolds for sustained release of SDF-1α, Int J Pharm 610 (2021) 121205. https://doi.org/10.1016/j.ijpharm.2021.121205.

[65] N.H. Ferreira, R. Molina-Pena, M. Najberg, C. Roy, L. Roncali, S. Avril, M.H. Mansor, F. Boury, C. Alvarez-Lorenzo, E. Garcion, P10.14.A Caught in a trap: Silk fibroin, hyaluronic acid, and heparin sponges to capture residual glioblastoma cells, Neuro Oncol 24 (2022) ii51–ii52. https://doi.org/10.1093/neuonc/noac174.179.

[66] Z.M. Khan, E. Wilts, E. Vlaisavljevich, T.E. Long, S.S. Verbridge, Characterization and structure-property relationships of an injectable thiol-Michael addition hydrogel toward compatibility with glioblastoma therapy, Acta Biomater 144 (2022) 266–278. https://doi.org/10.1016/j.actbio.2022.03.016.